PHYSICAL REVIEW B **84**, 125414 (2011)

Role of surface plasmon polaritons in the optical response of a hole pair

F. de León-Pérez,[1,2] F. J. García-Vidal,[3] and L. Martín-Moreno[2]

[1]*Centro Universitario de la Defensa de Zaragoza, Carretera de Huesca s/n, E-50090 Zaragoza, Spain*

[2]*Instituto de Ciencia de Materiales de Aragón and Departamento de Física de la Materia Condensada, CSIC-Universidad de Zaragoza, E-50009 Zaragoza, Spain*

[3]*Departamento de Física Teórica de la Materia Condensada, Universidad Autónoma de Madrid, E-28049 Madrid, Spain*

(Received 18 May 2011; published 7 September 2011)

The optical emittance of a hole pair perforated in an opaque metal film is studied from first principles using the coupled-mode method. The geometrical simplicity of this system helps us to understand the fundamental role played by surface plasmon polaritons (SPPs) in its optical response. A SPP interference model without fitting parameters is developed from the rigorous solution of Maxwell's equations. The calculations show that the interference pattern of the hole pair is determined by two scattering mechanisms: (i) the electric field excited by the external illumination at the hole openings before the hole-hole interaction is established and (ii) the re-illumination of the holes by the in-plane SPP radiation. The conditions for constructive and destructive interference only depend on the phase difference provided by each of the two scattering mechanisms.

DOI: 10.1103/PhysRevB.84.125414 PACS number(s): 73.20.Mf, 78.67.−n, 41.20.Jb

I. INTRODUCTION

The extraordinary transmission through nanohole arrays milled into metallic films[1] is attributed to the resonant excitation of surface electromagnetic (EM) modes by the incident light.[2] In the optical regime these surface EM modes are surface plasmon polaritons (SPPs) modified by the metal corrugation. The light-SPP coupling is made possible by the additional grating momentum provided by the scattering of the incident light by the hole array. Nevertheless, interference of excited SPPs is set up even for two interacting holes.[3–7] Increasing the number of holes, the transmission is enhanced due to better defined peaks of the structure factor, appearing at the reciprocal lattice vectors.[8] It must also be noted that light-SPP interaction is not the single mechanism behind the extraordinary optical transmission (EOT). The EOT physical scenario is completed by the excitation of localized and Fabry-Pérot modes,[9–16] which may also contribute the whole process (see Ref. 17 for a comprehensive review).

The aim of the present paper is to study the interference pattern of the simplest interacting system: a hole pair. Since the original proposition of the "nanogolf" effect by Sönninchsen *et al.*,[3] several groups have measured the optical interaction of two holes, see for example Refs. 6,7, and 18. These groups have used basic SPP resonant models in order to explain the characteristic optical transmittance of the hole dimer, which oscillates as a function of the hole-hole distance, with period equal to the SPP wavelength. These approaches have in common that the relevant scattering channels are assumed *ad hoc*: only SPP scattering channels are included in the final optical response.

In this paper we make no such assumption and solve Maxwell's equations from first principles using a coupled-mode method (CMM).[17,19] We shall consider the two possible radiative channels: freely propagating light radiated out-of-plane into the far field, and SPP power scattered along the metal plane. The out-of-plane power $P_{\rm rad}$, normalized to the power incident on the hole area, gives the far field transmittance T. This is the quantity commonly used to characterize EOT. However, to the best of our knowledge, the in-plane SPP power $P_{\rm SPP}$ has not yet been measured for a hole pair. We shall analyze the relevant scattering mechanisms for each radiative channel. Moreover, we shall derive, without fitting parameters, the conditions for constructive and destructive interference, hereafter conditions for interference (CI), that explain experimental interference patterns.[6,18]

The paper is organized as follows. In the next section we briefly review the CMM and give the expressions for $P_{\rm SPP}$ and $P_{\rm rad}$. The assumptions behind the CMM and some cumbersome mathematical formula are reported in the Appendix. For the sake of completeness, Sec. III summaries the emittance of a single hole. Section IV discusses the optical response of the hole pair. A subsection is devoted to clarify the scattering mechanisms dominating the conditions for interference. At the end we outline the main conclusions of the paper.

II. THEORETICAL FRAMEWORK

Figure 1 renders the hole-pair geometry studied in this paper. Two identical circular holes of radius r_h, separated by a distance R, are milled into an infinite metal film of thickness h and dielectric function $\epsilon_{\rm m}$. In general, the metal film lays on a substrate with dielectric constant ϵ, it is covered with a dielectric superstrate ϵ_1, and the space inside the holes is characterized by a dielectric constant ϵ_2. For the sake of simplicity, $\epsilon = \epsilon_1 = \epsilon_2 = 1$ is used in this paper. We consider in what follows that the metal film is illuminated by a normal-incident p-polarized plane wave, oriented along the main axis of the hole pair, as shown in Fig. 1. We shall focus on the energy power radiated into the transmission region ($z > 0$).

Maxwell's equations are solved self-consistently using a convenient representation for the EM fields.[17,19] In both substrate and superstrate the fields are expanded into an infinite set of plane waves with both p and s polarizations. Inside the holes the most natural basis is a set of circular waveguide modes. Convergence is fast achieved with a small number of such modes.[20,21] In fact, we shall see that the fundamental waveguide mode is a good approximation for our problem. The assumptions behind this coupled-mode method, as well

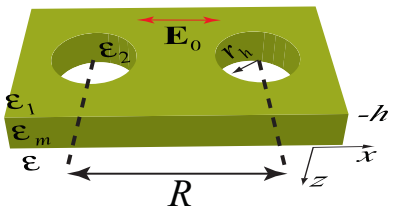

FIG. 1. (Color online) Schematic representation of the hole-pair geometry.

as its relevant constitutive quantities, are briefly reviewed in the Appendix under the single mode approximation.

The flux power traversing the hole is distributed into two channels[19]: (i) out-of-plane radiation, freely propagating into the far field, and (ii) SPP power, scattered along the metal plane. The calculation of these two quantities is straightforward within the CMM after we know the amplitude of the fundamental waveguide mode at the hole openings E'_i, where $i = 1,2$ labels each hole. For a normal-incident plane wave, both holes receive the same illumination I (A1), therefore $E'_1 = E'_2 \equiv E'$ due to the symmetry of the system with respect to the central point of the hole pair; E' hence reads

$$E' = \frac{G_v I}{[G_{\rm sh} + G_{hh}(R) - \Sigma]^2 - G_v^2}, \tag{1}$$

where the hole-hole propagator $G_{hh}(R)$ [Eq. (A4)] represents the coupling of the two holes as a function of the hole-hole distance R. This interaction can be seen as a re-illumination of the hole i by the magnetic field $G_{hh}E_j$ radiated from the other hole j. Notice that there is also a self-illumination term for each hole $G_{\rm sh}$, which adds to the single-hole scattering mechanisms represented by both Σ [Eq. (A2)] and G_v [Eq. (A3)]. Using Eq. (1), the out-of-plane power emitted by the hole pair simplifies to

$$P_{\rm rad}(R) = |E'|^2 g_{\rm rad}(R), \tag{2}$$

where the propagator $g_{\rm rad}(R) = g^{\rm sh}_{\rm rad} + g^{\rm int}_{\rm rad}(R)$ provides the far field radiated from the hole pair, $g^{\rm sh}_{\rm rad}$ represents the contribution of each single hole, and $g^{\rm int}_{\rm rad}(R)$ [Eq. (A8)] is a term arising from the interference of the fields radiated by the two holes.

On the other hand, we can obtain the power radiated into SPPs by computing the contribution from the plasmon pole in the propagator.[19] The power of the scattered SPPs is first computed at a point r on the metal surface several SPP wavelengths away from the nearest edge of the hole pair, by integrating the in-plane radial component of the Poynting vector, defined with the SPP fields, on a cylindrical surface of radius r and semi-infinity extension in $z > 0$; the power in the plasmon wave is then calculated using the known decay length of the SPP. The integrated power reads

$$P_{\rm SPP}(R) = |E'|^2 g_{\rm SPP}(R), \tag{3}$$

where the propagator $g_{\rm SPP}(R) = g^{\rm sh}_{\rm SPP} + g^{\rm int}_{\rm SPP}(R)$ provides the total SPP field radially scattered along all possible angular directions in the metal plane, $g^{\rm sh}_{\rm SPP}$ [Eq. (A11)] represents the contribution of each single hole, and $g^{\rm int}_{\rm SPP}(R)$ [Eq. (A12)] is the interference term

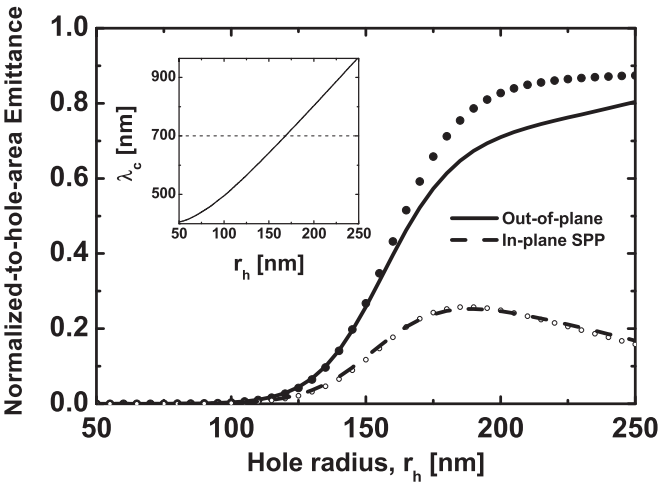

FIG. 2. Normalized-to-hole-area out-of-plane ($P_{\rm rad}$) and in-plane SPP ($P_{\rm SPP}$) emittance as function of the hole radius r_h (in nm) for a single hole milled in a silver film, free standing on air ($h = 250$ nm and $\lambda = 700$ nm). Symbols and lines represent converged results and the single mode approximation, respectively. The inset show the cutoff wavelength, λ_c (in nm).

Nevertheless, the hole-hole interaction can not be fully understood without a previous knowledge of the optical response of a single hole, which is briefly reviewed in the next section.

III. SINGLE HOLE EMITTANCE

The emittance spectrum of a single circular hole is described in this section for the sake of completeness, although this issue has been largely studied, see for example Refs. 3,9,10,14,15,18–23, and references therein. The behavior of both $P_{\rm rad}$ and $P_{\rm SPP}$ is depicted in Fig. 2 as function of the hole radius, for a free-standing Ag film with $h = 250$ nm. The Ag dielectric function $\epsilon_{\rm m}(\lambda)$ is fitted to data in Ref. 24. It is equal to $\epsilon_{\rm m} = -19.9 + 1.15\,i$ for the incident wavelength, $\lambda = 700$ nm, which is kept constant in the paper. Both $P_{\rm rad}$ and $P_{\rm SPP}$ are normalized to the power incident on the hole area.

Figure 2 renders $P_{\rm SPP}$ for both the fundamental mode approximation (dashed line) and converged results (open circles). Both curves practically overlap, so the fundamental mode is enough to achieve converged results for this emittance channel. For the out-of-plane emittance the agreement between single mode (solid line) and full calculations (full circles) is slightly worse, but still the difference is less than 15% and tendencies are well captured in the parameter range considered. The single mode approximation is therefore used in the rest of the paper.

As already stressed in Ref. 20, $P_{\rm SPP}(r_h)$ presents a broad peak with maximum at $r_h = 190$ nm, close to the cutoff radius, $r_{\rm c} = 168$ nm for $\lambda = 700$ nm. The cutoff wavelength $\lambda_{\rm c}$ is represented in the inset of Fig. 2 as a function of r_h. The resonance appears in the field at the opening $|E'|$ (not shown), while the decay for $r_h > r_{\rm c}$ is due to that in the single hole SPP propagator $g^{\rm sh}_{\rm SPP}$ [Eq. (A11)]. For $r_h > r_{\rm c}$ most of the the energy is radiated out of the plane. In this case, both $g^{\rm sh}_{\rm rad}$ (not shown) and $P_{\rm rad}$ reach a fast saturation with the hole radius.

IV. OPTICAL RESPONSE OF A HOLE PAIR

We define the *normalized* hole pair emittance as the power radiated into each channel, out-of-plane [Eq. (2)] or in-plane-SPP [Eq. (3)], divided by twice the corresponding emitted power of a single hole located at $R = 0$, that is,

$$\eta_{\rm rad}(R) = \frac{P_{\rm rad}(R)}{2P_{\rm rad}^{\rm sh}} = |E'_N|^2 g_{\rm rad}^{\rm N}(R), \tag{4}$$

$$\eta_{\rm SPP}(R) = \frac{P_{\rm SPP}(R)}{2P_{\rm SPP}^{\rm sh}} = |E'_N|^2 g_{\rm SPP}^{\rm N}(R), \tag{5}$$

where E'_N is the ratio of the electric field at the hole openings

$$E'_N(R) = \frac{E'(R)}{E'_{\rm sh}} = \frac{[G_{\rm sh} - \Sigma]^2 - G_v^2}{[G(R) - \Sigma]^2 - G_v^2}, \tag{6}$$

and we have used that the illumination of an isolated hole is equal to the illumination of each hole in the pair for a normal incident plane wave; while the ratios for the out-of-plane and SPP propagators are given by

$$g_{\rm rad}^{\rm N}(R) = \frac{g_{\rm rad}(R)}{g_{\rm rad}^{\rm sh}}, \tag{7}$$

$$g_{\rm SPP}^{\rm N}(R) = \frac{g_{\rm SPP}(R)}{g_{\rm SPP}^{\rm sh}}. \tag{8}$$

The normalized emittances $\eta_{\rm rad}$ and $\eta_{\rm SPP}$ are depicted in Fig. 3 as a function of the hole-hole distance R for increasing hole radius; $r_h = 100$ nm (blue dashed line), 150 nm (red solid line), and 250 nm (black short-dashed line). In Fig. 3 the interhole distance R is normalized to the SPP wavelength $\lambda_{\rm SPP} = 2\pi/{\rm Re}[k_{\rm SPP}]$, where $k_{\rm SPP}$ (A10) is the SPP propagation constant in silver; $\lambda_{\rm SPP} = 682.3$ nm for the chosen $\lambda = 700$ nm.

In accordance with experimental works,[6,7] the computed powers $\eta_{\rm rad}$ and $\eta_{\rm SPP}$ oscillate with period $\lambda_{\rm SPP}$. However, $\eta_{\rm rad}$ behaves different than $\eta_{\rm SPP}$ as a function of the hole radius. The amplitude of $\eta_{\rm rad}$ strongly oscillates with r_h, while $\eta_{\rm SPP}$ does not. Indeed, increasing r_h from 100 to 150 nm at fixed R we can transform a maximum of $\eta_{\rm rad}$ into a minimum. To the best of our knowledge this dependence of $\eta_{\rm rad}$ on r_h has not been previously reported. Moreover, in the thin-film limit it has been found that the CI only depend on the edge-edge distance, and not on r_h. Further experimental work is needed to study the dependence on r_h for opaque metal films and hole sizes larger that the metal skin depth (the region of the parameter space targeted in this paper). Nevertheless, it is worth stressing that the available experimental data[6,7] reported the same CI for very different systems.[25] In both cases r_h is very small ($\sim\lambda/20$), but while Ref. 6 considers a thin gold layer ($h =$ 20 nm) on a glass substrate, Ref. 7 uses an optically thick silver film immersed in a medium with refractive index $n = 1.45$. Both experimental CI are the same as for a third different system, the particular case $r_h = 150$ nm in Fig. 3(a), that is, maxima are at $R/\lambda_{\rm SPP} = m - 1/4$, minima at $R/\lambda_{\rm SPP} = m + 1/4$ (both represented with arrows), and $\eta_{\rm rad} = 1$ at $R/\lambda_{\rm SPP} = (m + 1)/2$ (represented with vertical dashed lines), where $m = 1,2,3,\ldots$.

In contrast, the amplitude of $\eta_{\rm SPP}$ shows a stronger dependence on R, but does not present such large variations

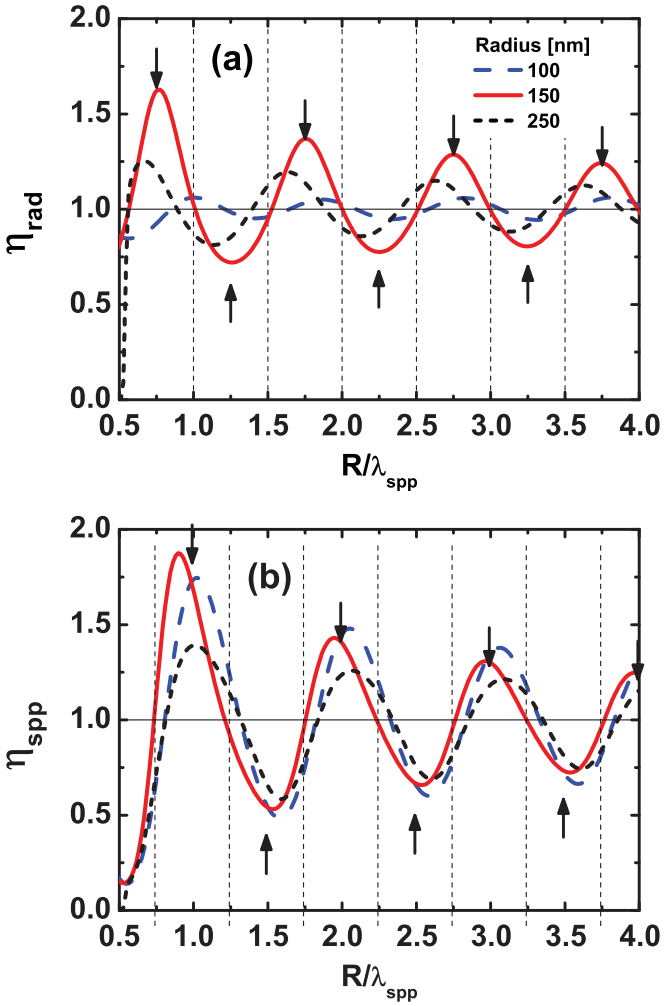

FIG. 3. (Color online) (a) Normalized out-of-plane emittance $\eta_{\rm rad}$ and (b) normalized in-plane SPP emittance $\eta_{\rm SPP}$ as function of $R/\lambda_{\rm SPP}$ for increasing r_h; $r_h = 100$ nm (blue dashed line), 150 nm (red solid line), and 250 nm (black short-dashed line). The holes are milled in a free standing Ag film of thickness = 250 nm. The illumination wavelength is $\lambda = 700$ nm. The CI reported in Sec. IV A are included in both (a) and (b) for $r_h = 150$ nm: maxima (at $R/\lambda_{\rm SPP} = m - 1/4$ for $\eta_{\rm rad}$ and $R/\lambda_{\rm SPP} \approx m$ for $\eta_{\rm SPP}$) and minima (at $R/\lambda_{\rm SPP} = m + 1/4$ for $\eta_{\rm rad}$ and $R/\lambda_{\rm SPP} \approx m - 1/2$ for $\eta_{\rm SPP}$) are represented with arrows, while vertical dashed lines are used for the condition $\eta = 1$ [at $R/\lambda_{\rm SPP} = (m + 1)/2$ for $\eta_{\rm rad}$ and $R/\lambda_{\rm SPP} \approx (2m + 1)/4$ for $\eta_{\rm SPP}$]; $m = 1,2,3,\ldots$.

with size of the holes. Maxima of $\eta_{\rm SPP}$ occur close to the conditions for constructive interference of SPPs at the flat metal surface ($R = m\lambda_{\rm SPP}$), while minima appear close to conditions for destructive interference of SPPs between the holes [$R = (2m - 1)\lambda_{\rm SPP}/2$].

As the energy traversing the holes is distributed into the out-of-plane and in-plane channels [Eq. (A15)], $\eta_{\rm rad}$ and $\eta_{\rm SPP}$ behave as complementary scattering channels, so they do not have the same kind of extreme value (a maximum, a minimum, or $\eta = 1$) at the same R. In particular, there is neither a transmission enhancement nor suppression of $\eta_{\rm rad}$ at the conditions for constructive interference of SPPs. Such counterintuitive behavior was stressed in Ref. 7, where experimental results

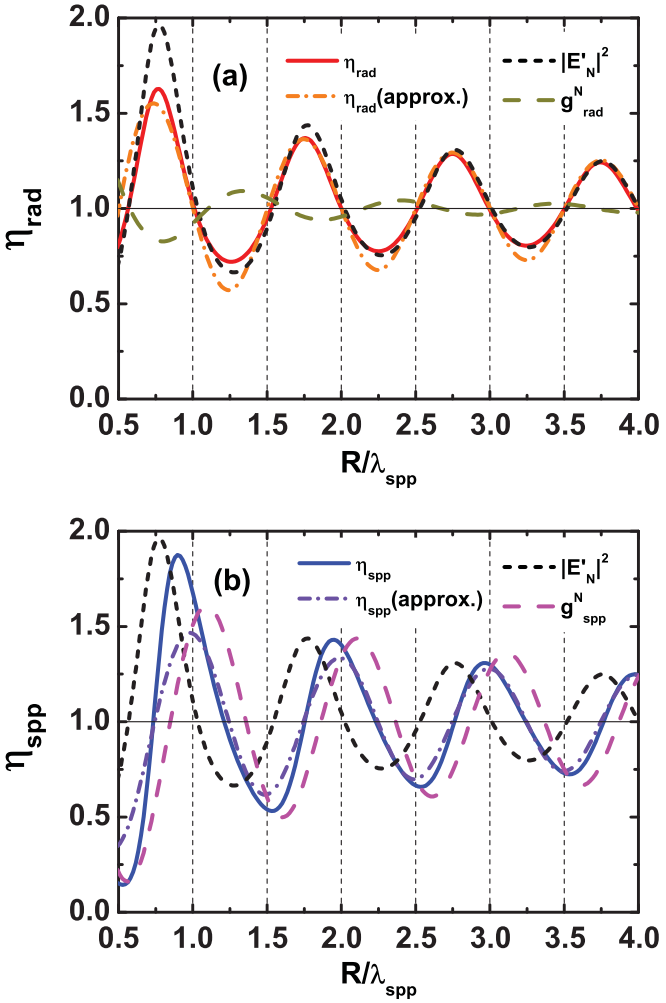

FIG. 4. (Color online) (a) Normalized out-of-plane emittance $\eta_{\rm rad}$ (red solid line), its constituent terms $|E'_N|^2$ (black short-dashed line), and $g^{\rm N}_{\rm rad}$ (dark-yellow dashed line), and the approximate expression for $\eta_{\rm rad}$ (orange dash-dotted line) of Eq. (10). (b) Normalized SPP emittance $\eta_{\rm SPP}$ (blue solid line), its constituent terms $|E'_N|^2$ (black short-dashed line) and $g^{\rm N}_{\rm SPP}$(magenta dashed line), and the approximate expression for $\eta_{\rm SPP}$ (violet dash-dotted line) of Eq. (14). All these quantities are represented as function $R/\lambda_{\rm SPP}$. The hole radius is $r_h = 150$ nm, the rest of parameters are the same as in Fig. 3.

have been nicely fitted to a SPP interference model although this data also shows that $\eta_{\rm rad} = 1$ at $R = m\lambda_{\rm SPP}$.

The out-of-plane radiation $\eta_{\rm rad}$ (4) is mainly determined by E'_N, that is, by the change in the field at the hole due to the presence of the other hole. This is illustrated in Fig. 4(a), where $\eta_{\rm rad}$ is compared with both $|E'_N|^2$ and $g^{\rm N}_{\rm rad}$. We observe that the interference between the radiative field of the two holes, given by $g^{\rm N}_{\rm rad}$, practically does not change the total transmission for hole-hole distances larger than $2\lambda_{\rm SPP}$. Conversely, the normalized in-plane propagator $g^{\rm N}_{\rm SPP}$ plays an important role setting up the CI for $\eta_{\rm SPP}$ (5), see Fig. 4(b). Although the contribution of $|E'_N|^2$ cannot be neglected, the interference pattern of $g^{\rm N}_{\rm SPP}$ resembles the behavior of $\eta_{\rm SPP}$.

The CI developed in the next section strongly depend on the properties of the in-plane propagator $G_{hh}(R)$, which is behind the interference pattern of both radiative channels. We use the following decomposition of the in-plane propagator:

$$G_{hh}(R) = G^{hh}_{\rm rad}(R) + G^{hh}_{\rm SPP}(R) + G^{hh}_{\rm ev}(R), \qquad (9)$$

where $G^{hh}_{\rm rad}(R)$ [Eq. (A8)] represents the contribution of radiative modes, $G^{hh}_{\rm SPP}(R)$ [Eq. (A9)] designates the contribution of the plasmon pole to evanescent modes, and $G^{hh}_{\rm ev}(R)$ [Eq. (A13)] denotes the contribution of the remaining evanescent modes. This decomposition is the most natural way of connecting G_{hh} [Eq. (A4)] to the radiative propagators $g_{\rm rad}$ [Eq. (2)] and $g_{\rm SPP}$ [Eq. (3)], as well as to recover previous results for the PEC.[8] Additionally, it is also related to the decomposition proposed in Ref. 26 in order to compare SPP with non-SPP mediated interaction.

The real and imaginary parts of $G^{hh}_{\rm rad}(R)$, $G^{hh}_{\rm ev}(R)$, and $G^{hh}_{\rm SPP}(R)$ are compared with $G_{hh}(R)$ in Fig. 5 for the same parameters of Fig. 4. The most relevant feature observed in Figs. 5(a) and 5(b) is that the main contribution to $G_{hh}(R)$ comes from the SPP propagator $G^{hh}_{\rm SPP}(R)$, which has a simple analytical form [Eq. (A9)]. This allows us to find analytical expression for CI that will be presented in the next section. Notice that the agreement between $G_{hh}(R)$ and $G^{hh}_{\rm SPP}(R)$ has been previously reported for 1D defects separated a distance larger that $2-3\lambda$.[27] Regarding non-SPP channels, $G^{hh}_{\rm rad}(R)$ decays faster than $G^{hh}_{\rm SPP}(R)$ being negligible small for R equal to a few $\lambda_{\rm SPP}$. On other hand, the real part of $G^{hh}_{\rm ev}(R)$ is vanishing small (see the Appendix), while its imaginary part is in antiphase to $G^{hh}_{\rm rad}(R)$. It must be noted that, as expected, the relative contribution of the different propagators changes when we approach the PEC limit.[26–29]

A. Conditions for interference

In this section we compute the conditions for constructive and destructive interference of both out-of-plane and in-plane radiative powers. We start with the simpler of these two quantities, $\eta_{\rm rad}$.

Three approximations simplify the study of $\eta_{\rm rad}$. First, its interference pattern is accurately described by the normalized square field amplitude $\eta_{\rm rad} \approx |E'_N|^2$, see Fig. 4(a). Second, $G_{hh}(R) \approx G^{hh}_{\rm SPP}(R)$, as we have learned from Fig. 5. Third, $G^{hh}_{\rm SPP}(R) \ll G_{\rm sh}$. This last approximation is valid for $R \gg \lambda_{\rm SPP}$, but we shall see it gives results that work surprisingly well even for $R \sim \lambda_{\rm SPP}$. Expanding E'_N (6) into Mclaurin series of $G^{hh}_{\rm SPP}(R)/G_{\rm sh}$ and keeping only the leading term, we find

$$E'_N = \frac{E'}{E'_{\rm sh}} \approx 1 - 2\,Z_E\,G^{hh}_{\rm SPP}(R),$$

where $Z_E = E_{\rm sh}/I$ [Eq. (A7)] is the effective impedance of a single hole, which gives the modal amplitude at the hole opening normalized by the external illumination. From the simplified expression for E'_N we can deduce that the interference pattern of the hole pair is set up by both the single hole impedance and the re-illumination of one hole by the other.

The CI for $\eta_{\rm rad}$ can be written in terms of the phase difference provided by both Z_E and $G^{hh}_{\rm SPP}(R)$. We thus define the single-hole phase shift, ϕ_{ZE}, from $Z_E = |Z_E|\exp(i\phi_{ZE})$, as well as the phase difference acquire by the SPP when traveling from one hole to the other, ϕ_{hh}, from

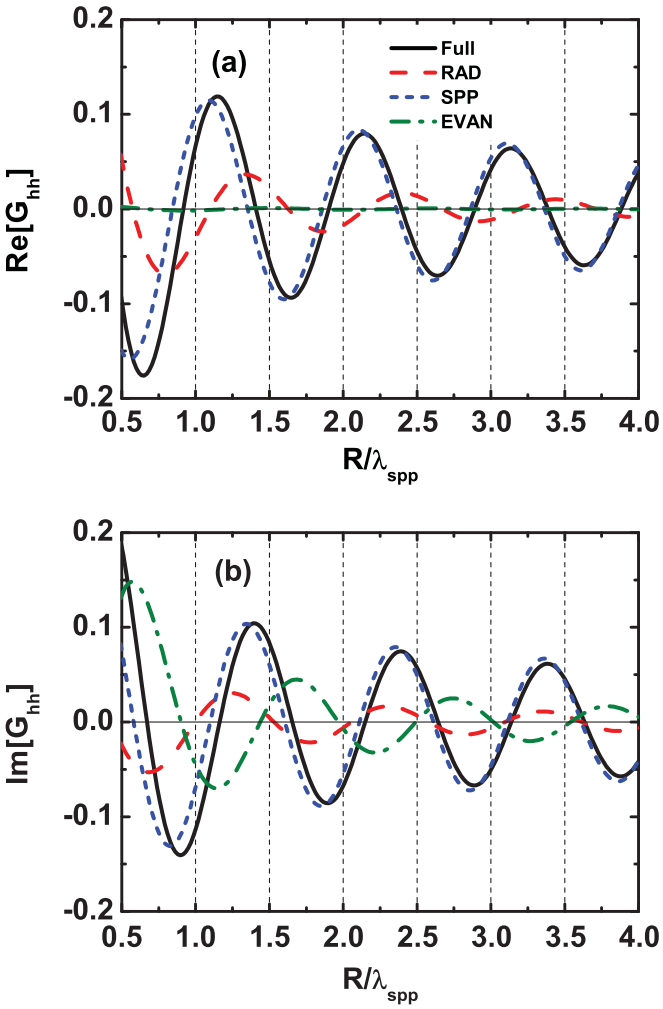

FIG. 5. (Color online) (a) Real and (b) imaginary parts of the propagator $G_{hh}(R)$ (black solid line), as well as its constituent terms for radiative modes, $G^{hh}_{\rm rad}(R)$ (red dashed line), SPP modes, $G^{hh}_{\rm SPP}(R)$ (blue short-dashed line), and remaining evanescent modes $G^{hh}_{\rm ev}(R)$ (green dash-dotted line). We use the same geometrical parameters of Fig. 4.

$G^{hh}_{\rm SPP}(R) = |G^{hh}_{\rm SPP}(R)| \exp(i\phi_{hh})$. An approximate expression for ϕ_{hh} can be obtained replacing the Hankel function in $G^{hh}_{\rm SPP}$ [Eq. (A9)] by its asymptotic expression $H_1^{\prime(1)}(x) \approx (\pi x/2)^{-1/2} \exp[i(x - \pi/4)]$. We have then $\phi_{hh} = k_{\rm SPP}R - \pi/4$. Keeping again the leading term in the expansion of $|E'_N|^2$, we obtain

$$\eta_{\rm rad} \approx 1 - 4\left|Z_E G^{hh}_{\rm SPP}\right| \cos(k_{\rm SPP}R + \phi_{ZE} - \pi/4). \quad (10)$$

This equation clearly shows that the out-of-plane radiation depends both on the phase picked up by the field given the illumination provided by the external field and on the optical path traveled by the SPP when going to one hole to the other.

The approximate equation (10) is compared with full calculations in Fig. 4(a). As $\eta_{\rm rad} \approx |E'_N|^2$, we find that Eq. (10) slightly underestimates $|E'_N|^2$ for $R < \lambda_{\rm SPP}$, but the agreement is excellent for $R > \lambda_{\rm SPP}$. This nice agreement is related to the fact that non-SPP waves at the metal plane decay faster than SPP waves as a function of the distance, see Fig. 5. The leading role of SPP waves for large R have been already stressed in Refs. 26–29. Equation (10) also agrees with the one proposed in Ref. 7 following an intuitive interference plasmon model, which, in contrast to first-principles derivation of (10), contains fitting parameters.

It is straightforward to derive the CI of $\eta_{\rm rad}$ from Eq. (10) assuming that the absolute value of $G^{hh}_{\rm SPP}$ changes smoothly with R, and that the dependence on R mainly comes from its phase. Then we have that extrema of $\eta_{\rm rad}$ appear at

$$k_{\rm SPP}R - \frac{\pi}{4} + \phi_{ZE} = n\pi, \quad (11)$$

where the integer value of n is equal to $n = 2m - 1$ for maxima, $n = 2m$ for minima, and $m = 1,2,3,\ldots$; while the condition for $\eta_{\rm rad} = 1$ is shifted in $\pi/2$ with respect to the previous expression, that is,

$$k_{\rm SPP}R - \frac{\pi}{4} + \phi_{ZE} = \left(m + \frac{1}{2}\right)\pi. \quad (12)$$

The single-hole phase shift ϕ_{ZE} is depicted in Fig. 6(a) as function of the of the hole radius r_h, and for increasing metal thickness $h = 100$ nm (blue dashed line), 150 nm (red solid line), and 250 nm (black short-dashed line).

The large variation in ϕ_{ZE} as function of r_h (up to $\pi/2$ for increasing r_h from 50 to 250 nm) accounts for the oscillations in $\eta_{\rm rad}$ observed in Fig. 3(a). As an example, we choose in Fig. 6(a) the point $r_h = 150$, $h = 250$ nm, for which $\phi_{ZE} = -\pi/4$. Equations (11) and (12) give simple expressions for this specific value of ϕ_{ZE}. We thus obtain maxima of $\eta_{\rm rad}$ at $R/\lambda_{\rm SPP} = m - 1/4$, minima at $R/\lambda_{\rm SPP} = m + 1/4$, and $\eta = 1$ at $R/\lambda_{\rm SPP} = (m + 1)/2$, with $m = 1,2,3,\ldots$. We compare these CI with full calculations in Fig. 3(a). An excellent agreement is obtained even for small values of $R/\lambda_{\rm SPP}$. The same agreement is observed for any given value of r_h (not shown).

It is also worth to say that $\eta_{\rm rad}$ is largely independent on the metal thickness h (although it is computed for a given value of of h in optically thick film) because ϕ_{ZE} is practically independent on h, see Fig. 6.

Notice that the CI represented by Eqs. (11) and (12), which are valid for a wide range of hole sizes (larger than the metal skin depth) and opaque metal films, are expressed in terms of the distance between the centers of the holes. A previous work[6] suggested that, for thin-metal films and small hole sizes, the CI are a function of the edge-edge distance, independently from the hole radius. In our notation, this could only occurs if $\phi_{ZE} + 2r_h/\lambda_{\rm SPP} = 0$ in Eq. (10). However, we observe in Fig. 6(a) that $-2r_h/\lambda_{\rm SPP}$ (dash-dotted line) is equal to ϕ_{ZE} only for a small region of the parameter space. This novel behavior demands further experimental work on opaque metal films and hole sizes larger than the metal skin depth.

Similar CI can be developed for the in-plane scattered power $\eta_{\rm SPP}$. As commented in the discussion of Fig. 4(b), both terms $|E'_N|^2$ and $g^{\rm N}_{\rm SPP}$ contribute to $\eta_{\rm SPP}$ in Eq. (5). We take the approximate expression of $|E'_N|^2$ from Eq. (10) and use the asymptotic expression $g^{\rm N}_{\rm SPP} = 1 + 2J_1'(k_{\rm SPP}R)$ found in the Appendix. We recall that the last relation is exact only when absorption is neglected, but it is a good approximation if absorption is present. Using again the asymptotic expansion of

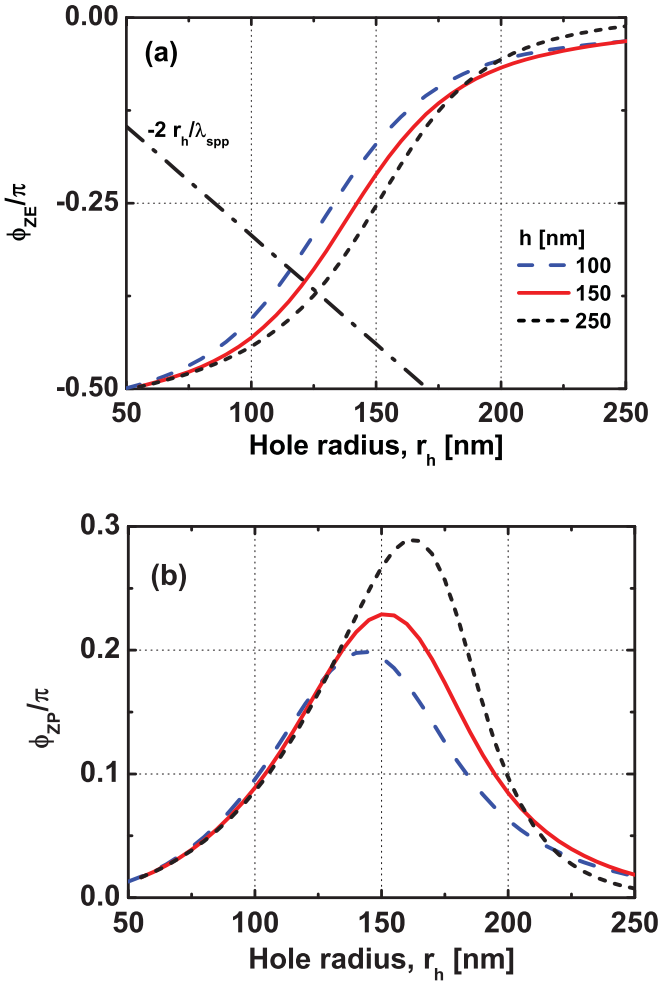

FIG. 6. (Color online) (a) Single-hole phase shift for the out-of-plane emittance ϕ_{ZE} as function of the hole radius r_h and for increasing metal thickness h; $h = 100$ nm (blue dashed line), 150 nm (red solid line), and 250 nm (black short-dashed line). The dash-dotted line represents the hole diameter normalized by λ_{SPP}. (b) SPP phase shift for the in-plane emittance of a single hole ϕ_{ZP}.

the Bessel function, the in-plane emittance is thus simplified to

$$\eta_{SPP} \approx |E'|^2 \left[1 + 2\sqrt{\frac{2}{\pi k_{SPP} R}} \cos(k_{SPP} R - \pi/4)\right]. \quad (13)$$

This equation tells us that, given the normalized amplitude of the electric field at the hole opening E'_N, the interference pattern of the in-plane scattering power is determined by the SPP optical path between the two holes. However, in order to quantify the CI of η_{SPP}, we should include the modulation of the field given by $|E'_N|^2$ [Eq. (10)]. Expanding the two terms in Eq. (13) up to the first order in G^{hh}_{SPP}/G_{sh}, η_{SPP} can be straightforwardly rewritten to

$$\eta_{SPP} \approx 1 + 4\left|Z_{SPP} G^{hh}_{SPP}\right| \cos(k_{SPP} R + \phi_{ZP} - \pi/4), \quad (14)$$

where the effective impedance for the SPP channel $Z_{SPP} = Z_E - (4|G^{sh}_{SPP}|)^{-1}$ takes into account both the excitation of the EM field inside the hole, characterized by Z_E, and the excitation of the SPP at the hole, given by $(4|G^{sh}_{SPP}|)^{-1}$. Like for the out-of-plane channel, the approximate Eq. (14) shows an excellent agreement with full calculations in Fig. 4(b). However, the behavior of ϕ_{ZP} (defined from $Z_{SPP} = |Z_{SPP}|e^{i\phi_{ZP}}$) differs from ϕ_{ZE}. Figure 6(b) renders ϕ_{ZP} as a function of r_h, showing a characteristic peak centered near the cutoff radius $r_c = 168$ nm, cf. Fig. 2. The phase difference with respect to ϕ_{ZE} is about $\pi/2$ for $r_h \leqslant r_c$, and decreases to zero for $r_h > r_c$.

The extreme values of η_{SPP} (14) satisfy

$$k_{SPP} R - \frac{\pi}{4} + \phi_{ZP} = n\pi, \quad (15)$$

where the integer value of n is equal to $n = 2m$ for maxima, $n = 2m - 1$ for minima, and $m = 1,2,3,\ldots$. Notice that the values of $n\pi$ for η_{SPP} are shifted in π with respect to the extreme values of η_{rad} (conditions for maxima are replaced by conditions for minima, and vice versa). This shifting is determined by the fact that the power traversing the hole is radiated into two complementary channels: η_{rad} and η_{SPP}. As for η_{rad}, the condition $\eta_{SPP} = 1$ is shifted in $\pi/2$ with respect to the previous expression for extreme values, that is,

$$k_{SPP} R - \frac{\pi}{4} + \phi_{ZP} = \left(n + \frac{1}{2}\right)\pi. \quad (16)$$

In Fig. 3(b) we compare full calculations with the CI for the case $r_h = 150$ nm, $h = 250$ nm, for which $\phi_{ZP} = 0.27$ rad $\approx \pi/4$ [see Fig. 6(b)]. As for η_{rad}, an excellent agreement is obtained. Similar trends are found for $r_h = 100$ and 250 nm (not shown).

V. CONCLUSIONS

We have studied the emission pattern of a hole pair, focusing our attention in the role played by SPP resonances. Starting from the rigorous solution of the problem, we have developed a SPP interference model that does not contain fitting parameters. This model provides simple analytical expressions for the interference pattern of both the out-of-plane and in-plane radiation channels, which nicely agree with full calculations for noble metals at optical frequencies.

In agreement with experimental reports, both radiated powers oscillate with period λ_{SPP}. However, they show different trends as a function of the hole-hole distance and the hole radius. The amplitude of η_{rad} strongly oscillates with the hole radius, while the amplitude of η_{SPP} has a stronger dependence on R, but does not present such large variations with the hole size.

Maxima of η_{SPP} occur close to the conditions for constructive interference of SPPs at the flat metal surface ($R = m\lambda_{SPP}$), while minima appear close to conditions for destructive interference of SPPs between the holes [$R = (2m - 1)\lambda_{SPP}/2$]. The quantities η_{SPP} and η_{rad} have complementary conditions for constructive and destructive interference, because the power traversing the hole is distributed into these two channels.

We have also shown that two scattering mechanisms determine the interference pattern of the hole pair: (i) the electric field excited by the external illumination at the hole openings before the hole-hole interaction is established and (ii) the re-illumination of the holes by the in-plane SPP radiation. The conditions for interference only depend on the phase

difference provided by each of the two scattering mechanisms. The first mechanism is quantified by an effective impedance, with a given single-hole phase; while the additional phase provided by the second mechanism is just the optical path of the SPP traveling from one hole to the other. Our model explains that the oscillations of $\eta_{\rm rad}$ as a function of the hole size are due to the large variation in the effective impedance of the single hole.

ACKNOWLEDGMENTS

The authors gratefully acknowledge financial support from the Spanish Ministry of Science and Innovation under Grants MAT2009-06609-C02, CSD2007-046-NanoLight.es, and AT2009-0027.

APPENDIX: COUPLED-MODE METHOD

In this section we briefly review the coupled-mode method for the optical transmission through holes, under the fundamental waveguide mode (TE_{11}) approximation. We refer to Ref. 19 for the expressions of the full multimode formalism and their derivation. Within the CMM, Maxwell's equations are solved self-consistently using a convenient representation for the EM fields. In both substrate and superstrate (see Fig. 1), the fields are expanded into an infinite set of plane waves with both p and s polarizations. Inside the holes the most natural basis is a set of circular waveguide modes.[30] The parallel components of the fields are matched at the metal/dielectric interface using surface impedance boundary conditions (SIBCs).[31] Although SIBCs neglect the tunneling of EM energy between the two metal surfaces, this effect is not relevant for a metal thickness larger than a few skin depths.

At the lateral walls of the holes we choose the PEC approximation for the sake of analytical simplicity. We are thus neglecting absorption losses at the walls. Nevertheless, we upgrade the PEC approximation introducing two phenomenological corrections. First, the propagation constant of the PEC fundamental mode is replaced by the one computed for a real metal. This improves the comparison between CMM and both experimental and FDTD results for both the spectral position of the peaks and the dependence of optical properties on the metal thickness. Second, enlarging the radius of the hole by one skin depth simulates the real penetration of in field into the metallic walls. This value for the enlargement provides the best agreement with FDTD simulations for an infinite periodic array of holes.[21]

After matching the fields at the interface we arrive to the following system of tight binding-like equations:

$$[G_{\rm sh}-\Sigma]E_1(R)+G_{hh}(R)E_2(R)-G_v E_1'(R)=I_1,$$
$$[G_{\rm sh}-\Sigma]\,E_1'(R)+G_{hh}(R)E_2'(R)-G_v E_2'(R)=0,$$

where E_i is the modal amplitude of the electric field at the input opening of the ith hole, $i=1,2$, and E_i' is the same quantity but at the output opening. Two additional equivalent equations are needed for E_2 and E_2'. Other relevant quantity is the illumination provided by the normal-incident p-polarized plane wave, with wave number $k_\lambda=2\pi/\lambda$ and admittance $Y_0=\sqrt{\epsilon_1}$, onto the lowest energy mode

$$I\equiv I_1=I_2=\frac{\sqrt{2Y_0}}{1+z_sY_0}\frac{k_\lambda}{\sqrt{u^2-1}}, \tag{A1}$$

where $z_s=\epsilon_m^{-1/2}$ is the metal impedance. In order to obtain a transmittance normalized by the flux impinging on the area covered by the holes, the illumination term I already contains a factor $(\pi r_h^2 Y_0)^{-1/2}$. The constant u satisfies $J_1'(u)=0$,[30] where $J(x)$ is the Bessel function of order 1, and the prime denotes derivation with respect to its argument

The quantities Σ and G_v represent scattering mechanisms already present in single holes. Σ is related to the bouncing back and forth of the waveguide fields inside the holes. Its value is

$$\Sigma=Y_w\frac{f_w^+\,\mathrm{e}^{ik_zh}+f_w^-\,\mathrm{e}^{-ik_zh}}{f_w^{+2}\,\mathrm{e}^{ik_zh}-f_w^{-2}\,\mathrm{e}^{-ik_zh}}, \tag{A2}$$

where k_z is the propagation constant of the waveguide mode, h is the metal thickness, $f_w^\pm=1\pm z_sY_w$, $Y_w=k_z/k_{\epsilon_2}$ is the admittance for the excited TE_{11} mode, and $k_{\epsilon_2}=\sqrt{\epsilon_2}k_\lambda$. The quantity

$$G_v=2Y_w\left(f_w^{+2}\,\mathrm{e}^{ik_zh}-f_w^{-2}\,\mathrm{e}^{-ik_zh}\right)^{-1} \tag{A3}$$

reflects the coupling between EM fields at the two sides of a given hole.[19]

The propagator $G_{hh}(R)$ represents the coupling of the two holes. It results from the projection of the Green's dyadic onto the waveguide modes in the holes. For the TE_{11} mode, G_{hh} can be written as the following integral in the plane of the reciprocal space parallel to the metal surface:

$$G_{hh}(R)=G_0\int_0^\infty\left[\frac{G_p(q)}{q_z+z_s'}+\frac{G_s(q)}{q_z^{-1}+z_s'}\right]qdq, \tag{A4}$$

where $G_0=4k_\epsilon^2r_h^2\sqrt{\epsilon}/(u^2-1)$ and the two terms in the integrand represent the contribution of p- and s-polarized plane waves in the infinite semispace in contact with the metal surface. The denominators of these two terms stand for the response of the metal plane. In particular, the p term has a pole at the SPP wave vector. The numerators G_p and G_s account for both the single hole response, which is a function of the hole radius r_h, and the hole-hole interaction, a function of R. They read

$$G_p(q,r_h,R)=\frac{J_1^2(k_\epsilon q r_h)}{k_\epsilon^2q^2r_h^2}J_1'(k_\epsilon qR), \tag{A5}$$

$$G_s(q,r_h,R)=\frac{J_1'^2(k_\epsilon q r_h)}{\left(1-\frac{k_\epsilon^2q^2r_h^2}{u^2}\right)^2}\frac{J_1(k_\epsilon qR)}{k_\epsilon qR}. \tag{A6}$$

The integrand is written in adimensional units normalizing the wave vector by $k_\epsilon=k_\lambda\sqrt{\epsilon}$. Notice that the R-dependent Bessel functions are obtained after the angular integration in the $\mathbf{k}_\parallel=k_\epsilon q(\cos\theta,\sin\theta)$ plane, where θ defines the direction of the component of wave vector parallel to the metal plane $\mathbf{k}_\parallel$. The dielectric constant ϵ characterizes the dielectric material in contact with the metal surface (see Fig. 1, $\epsilon=\epsilon_1=1$ is used in this paper).

The self-interaction term $G_{\rm sh}$ is obtained after tacking the limit $R \to 0$ in $G_{hh}(R)$, that is, using the identities $\lim_{x\to 0} J_1'(x) = \lim_{x\to 0} J_1(x)/x = 1/2$.

Another relevant function is the effective impedance Z_E, which is determined by the the three scattering mechanisms of the single hole ($G_{\rm sh}$, G_v, and Σ),

$$Z_E = \frac{E_{\rm sh}}{I} = \frac{G_{\rm sh} - \Sigma}{(G_{\rm sh} - \Sigma)^2 - G_v^2}. \tag{A7}$$

We compute G_{hh} using the decomposition $G_{hh} = G_{\rm rad}^{hh} + G_{\rm SPP}^{hh} + G_{\rm ev}^{hh}$ (9), where $G_{\rm rad}^{hh}(R)$ represents the contribution of radiative modes, $G_{\rm SPP}^{hh}(R)$ designates the contribution of the plasmon pole to evanescent modes, and $G_{\rm ev}^{hh}(R)$ denotes the contribution of the remaining evanescent modes. The contribution of $G_{\rm rad}^{hh}(R)$ can be written in terms of the functions $g_{\rm rad}^{\rm int}(R)$ and $\Delta G_{\rm rad}^{hh}(R)$, which always take real values,

$$G_{\rm rad}^{hh}(R) = g_{\rm rad}^{\rm int}(R) + z_s'^{*}\Delta G_{\rm rad}^{hh}(R),$$

where

$$g_{\rm rad}^{\rm int}(R) = G_0 \int_0^1 dq \left(\frac{q q_z G_p}{|q_z + z_s'|^2} + \frac{q q_z G_s}{|1 + q_z z_s'|^2} \right) \tag{A8}$$

provides the interference term of the far field radiated from the holes (2), while the term proportional to the metal impedance z_s' reads

$$\Delta G_{\rm rad}^{hh}(R) = G_0 \int_0^1 q dq \left(\frac{G_p}{|q_z + z_s'|^2} + \frac{q_z^2 G_s}{|1 + q_z z_s'|^2} \right).$$

Both integrals are computed for free-propagating states ($0 \leqslant q \leqslant 1$). The real part of z_s' is very small for typical noble metals, making $\mathrm{Re}[G_{\rm rad}^{hh}] \approx g_{\rm rad}^{\rm int}$ and $\mathrm{Im}[G_{\rm rad}^{hh}] \approx |z_s| \Delta G_{\rm rad}^{hh}$ a good approximation for $G_{\rm rad}^{hh}$. The same relations hold for the single hole propagator $G_{\rm rad}^{sh}$.

For nonpropagating states ($q > 1$) the integrand in $G_{hh}(R)$ is prolonged into the complex q plane, see Ref. 19 for details. The residue of the Cauchy integral gives the SPP wave confined to the metal/air interface

$$G_{\rm SPP}^{hh} = \pi i z_s' G_0 \frac{J_1^2(k_{\rm SPP} r_h)}{k_{\rm SPP}^2 r_h^2} H_1'^{(1)}(k_{\rm SPP} R), \tag{A9}$$

where $k_{\rm SPP}$ is the parallel component of the SPP wave vector

$$k_{\rm SPP} = k_\epsilon \left[\frac{\epsilon\, \epsilon_{\rm m}(\lambda)}{\epsilon_{\rm m}(\lambda) + \epsilon} \right]^{1/2}. \tag{A10}$$

Equation (A10) defines $k_{\rm SPP}$ for a real metal and rigorous boundary condition at the metal/dielectric interface. In order to improve the accuracy of our model we use Eq. (A10) instead of the approximate SPP wave vector for SIBCs, $k_{\rm SPP}^{\rm SIBC} = k_\epsilon[\epsilon(1 - \epsilon_{\rm m}^{-1})]^{1/2}$. Besides the coupling propagator $G_{\rm SPP}^{hh}$, we define the radiative propagator $g_{\rm SPP}$, which provides the total SPP field radially scattered along all possible angular directions in the metal plane (3). We have that $g_{\rm SPP} = g_{\rm SPP}^{\rm sh} + g_{\rm SPP}^{\rm int}$, where the single-hole contribution read

$$g_{\rm SPP}^{\rm sh} = \frac{\pi |z_s'| |a_1| G_0}{2} \left| \frac{J_1(k_{\rm SPP} r_h)}{k_{\rm SPP} r_h} \right|^2, \tag{A11}$$

and the interference term is equal to

$$g_{\rm SPP}^{\rm int}(R) = g_{\rm SPP}^{\rm sh}\left[2\mathrm{Re}\left[J_1'(k_{\rm SPP}R)\right] + J_1'(2i\,\mathrm{Im}[k_{\rm SPP}R]) - \tfrac{1}{2}\right], \tag{A12}$$

while $a_1 = |k_{\rm zp}|\mathrm{Re}[k_{\rm SPP}]/(\mathrm{Im}[k_{\rm zp}]|k_{\rm SPP}|)$, and $k_{\rm zp} = (k_\epsilon^2 - k_{\rm SPP}^2)^{1/2}$. Notice that $g_{\rm SPP}^{\rm N} = g_{\rm SPP}^{\rm int}/g_{\rm SPP}^{\rm sh}$ (8) is independent of r_h.

For the sake of convenience, the integral for non-SPP evanescent states is computed along the vertical contour $q = 1 + ih \equiv q_+$, $h \in [0,\infty)$, after the integral variable is changed from q to h

$$G_{\rm ev}^{hh} = \frac{G_0}{2} \int_0^\infty q_+ dh \left(\frac{G_p}{\kappa_z - i z_s'} - \frac{G_p^*}{\kappa_z^* - i z_s'} - \frac{\kappa_z G_s}{1 + i z_s' \kappa_z} + \frac{\kappa_z^* G_s^*}{1 + i z_s' \kappa_z^*} \right), \tag{A13}$$

where $\kappa_z = \sqrt{2ih - h^2}$, and the Bessel function $J_1(x)$ in both G_p (A5) and G_s (A6) is replaced by a Hankel function of the first kind $H_1^{(1)}(x)$.

The propagator G_{hh} is further simplified when the metal absorption is neglected, that is, for $\mathrm{Im}[\epsilon_{\rm m}] = \mathrm{Re}[z_s'] = 0$ and $\mathrm{Im}[z_s'] = -|z_s'|$. We find for the radiative modes that $\mathrm{Re}[G_{\rm rad}^{hh}] = g_{\rm rad}^{\rm int}$, and $\mathrm{Im}[G_{\rm rad}^{hh}] = |z_s| \Delta G_{\rm rad}^{hh}$, while for SPP modes $\mathrm{Re}[G_{\rm SPP}(R)] = g_{\rm SPP}(R) = g_{\rm SPP}^{\rm sh}[1 + 2J_1'(k_{\rm SPP}R)]$. For the remaining evanescent modes we obtain that $G_{\rm ev}^{hh}$ is a pure imaginary function. The same relations that hold for G_{hh} are valid for $G_{\rm sh}$. Therefore, only the radiative and SPP terms contribute to the real part of in-plane propagator,

$$\mathrm{Re}[G_{\rm sh} + G_{hh}(R)] = g_{\rm rad}(R) + g_{\rm SPP}(R). \tag{A14}$$

Under the lossless metal approximation, the total power traversing the two holes simplifies to $P_{\rm hole} = \mathrm{Re}[G_v E E'^*]$.[19] We rewrite it in terms of E' with help of the relation $G_v E = [G_{\rm sh} + G_{hh}(R) - \Sigma]\, E'$, that is,

$$P_{\rm hole} = |E'|^2 \mathrm{Re}[G_{\rm sh} + G_{hh}(R)].$$

As Σ (A2) is purely imaginary for a lossless media, this term does not contribute to $P_{\rm hole}$. Using (A14) we then have

$$P_{\rm hole} = P_{\rm rad} + P_{\rm SPP}. \tag{A15}$$

This equality represents the conservation of the power flux traversing the hole. These results can be easily generalized to an arbitrary number of holes, waveguide modes, and noncylindrical geometries. It is also worth to mention that including absorption the computed powers differ in less than 5% from the lossless case, even for a large number of defects.[19–21]

Finally, we recall that PEC is a particular case of a lossless metal with $z_s' = 0$. In this case $G_{\rm rad}^{hh} = g_{\rm rad}^{\rm int}$, while for nonpropagating states of a PEC only $G_{\rm ev}^{hh}$ survives because $G_{\rm SPP}^{hh} = 0$.[8]

[1]T. W. Ebbesen, H. J. Lezec, H. F. Ghaemi, T. Thio, and P. A. Wolff, Nature (London) **391**, 667 (1998).
[2]L. Martín-Moreno, F. J. García-Vidal, H. J. Lezec, K. M. Pellerin, T. Thio, J. B. Pendry, and T. W. Ebbesen, Phys. Rev. Lett. **86**, 1114 (2001).
[3]C. Sönnichsen, A. C. Duch, G. Steininger, M. Koch, G. von Plessen, and J. Feldmann, Appl. Phys. Lett. **76**, 140 (2000).
[4]H. F. Schouten, N. Kuzmin, G. Dubois, T. D. Visser, G. Gbur, P. F. A. Alkemade, H. Blok, G. W. t Hooft, D. Lenstra, and E. R. Eliel, Phys. Rev. Lett. **94**, 053901 (2005).
[5]P. Lalanne, J. P. Hugonin, and J. C. Rodier, Phys. Rev. Lett. **95**, 263902 (2005).
[6]Y. Alarverdyan, B. Sepúlveda, L. Eurenius, E. Olsson, and M. Käll, Nat. Phys. **3**, 884 (2007).
[7]D. Pacifici, H. J. Lezec, L. A. Sweatlock, R. J. Walters, and H. A. Atwater, Opt. Express **16**, 9222 (2008).
[8]J. Bravo-Abad, F. J. García-Vidal, and L. Martín-Moreno, Phys. Rev. Lett. **93**, 227401 (2004).
[9]R. Wannemacher, Opt. Commun. **195**, 107 (2001).
[10]F. J. García de Abajo, Opt. Express **10**, 1475 (2002).
[11]A. Degiron, H. Lezec, N. Yamamoto, and T. Ebbesen, Opt. Commun. **239**, 61 (2004).
[12]F. J. García-Vidal, E. Moreno, J. A. Porto, and L. Martín-Moreno, Phys. Rev. Lett. **95**, 103901 (2005).
[13]K. L. van der Molen, K. J. K. Koerkamp, S. Enoch, F. B. Segerink, N. F. van Hulst, and L. Kuipers, Phys. Rev. B **72**, 045421 (2005).
[14]E. Popov, N. Bonod, M. Nevière, H. Rigneault, P.-F. Lenne, and P. Chaumet, Appl. Opt. **44**, 2332 (2005).
[15]F. J. García-Vidal, L. Martín-Moreno, E. Moreno, L. K. S. Kumar, and R. Gordon, Phys. Rev. B **74**, 153411 (2006).
[16]T. Rindzevicius, Y. Alaverdyan, B. Sepúlveda, T. Pakizeh, M. Käll, R. Hillenbrand, J. Aizpurua, and F. J. G. de Abajo, J. Phys. Chem. C **111**, 1207 (2007).
[17]F. J. García-Vidal, L. Martín-Moreno, T. W. Ebbesen, and L. Kuipers, Rev. Mod. Phys. **82**, 729 (2010).
[18]J. Alegret, P. Johansson, and M. Käll, New J. Phys. **10**, 105004 (2008).
[19]F. de León-Pérez, G. Brucoli, F. J. García-Vidal, and L. Martín-Moreno, New J. Phys. **10**, 105017 (2008).
[20]A. L. Baudrion, F. de León-Pérez, O. Mahboub, A. Hohenau, H. Ditlbache, F. J. García-Vidal, J. Dintinger, T. W. Ebbesen, L. Martín-Moreno, and J. R. Krenn, Opt. Express **16**, 3420 (2008).
[21]F. Przybilla, A. Degiron, C. Genet, T. W. Ebbesen, F. de Léon-Pérez, J. B.-A. J, F. J. García-Vidal, and L. Martín-Moreno, Opt. Express **16**, 9571 (2008).
[22]S.-H. Chang, S. K. Gray, and G. C. Schatz, Opt. Express **13**, 3150 (2005).
[23]A. Y. Nikitin, F. J. García-Vidal, and L. Martín-Moreno, Phys. Rev. Lett. **105**, 073902 (2010).
[24]P. B. Johnson and R. W. Christy, Phys. Rev. B **6**, 4370 (1972).
[25]The conditions for interference of Ref. 6 are given as function of the edge-edge distance. In order to rewrite it as a function of R one should take into account that $2r_h \approx \lambda_{SPP}/4$ for the measured r_h and wavelength.
[26]P. Lalanne and J. P. Hugonin, Nat. Phys. **2**, 551 (2006).
[27]F. López-Tejeira, F. J. García-Vidal, and L. Martín-Moreno, Phys. Rev. B **72**, 161405 (2005).
[28]T. Søndergaard and S. I. Bozhevolnyi, Phys. Rev. B **69**, 045422 (2004).
[29]H. Liu and P. Lalanne, Nature (London) **452**, 728 (2008).
[30]J. A. Stratton, *Electromagnetic Theory* (McGraw-Hill, New York, 1941).
[31]J. D. Jackson, *Classical Electrodynamics*, 3rd ed. (John Wiley, New York, 1999).